

Removal of Technetium (^{99}Tc) from Aqueous Waste by Manganese Oxide Nanoparticles Loaded into Activated Carbon

W. M. Abdellah^{1*}, H. I. El-Ahwany², R. El-Sheikh²

¹Radiation Protection Department, Egypt Nuclear and Radiological Regulatory Authority, Cairo, Egypt

²Chemistry Department, Faculty of Science, Zagazig University, Zagazig, Egypt

Email: *wmsra@yahoo.com

How to cite this paper: Abdellah, W.M., El-Ahwany, H.I. and El-Sheikh, R. (2020) Removal of Technetium (^{99}Tc) from Aqueous Waste by Manganese Oxide Nanoparticles Loaded into Activated Carbon. *Journal of Analytical Sciences, Methods and Instrumentation*, 10, 12-35.

<https://doi.org/10.4236/jasmi.2020.101002>

Received: January 23, 2020

Accepted: March 7, 2020

Published: March 10, 2020

Copyright © 2020 by author(s) and Scientific Research Publishing Inc. This work is licensed under the Creative Commons Attribution International License (CC BY 4.0).

<http://creativecommons.org/licenses/by/4.0/>



Open Access

Abstract

Technetium-99 is a radioactive isotope with a half-life of 2.13×10^5 year. ^{99}Tc is a significant contaminant of concern to the world. For this reason, a detailed understanding of technetium chemistry is essential for the protecting the public and the environment especially after increasing the various applications and uses of isotopes in the medical practices. Therefore, treatment of waste increases prior to the safe discharge to the environment or the storage. The sorption of technetium in the form of pertechnetate on a nano manganese oxide loaded into activated carbon has been investigated. Nano manganese oxide (NMO) was synthesized from manganese chloride and potassium permanganate by co-precipitation and forming a new composite by loading a nanoparticle into a modified activated carbon by different ratios. Modifications of activated carbons using different concentrations of HNO_3 (4 M, 6 M and 8 M) are used in prepared composites. Fourier transform infrared spectroscopy (FT-IR), X-Ray Diffraction (XRD) and Scanning Electron Microscope (SEM) were used to characterize the prepared composites. The adsorption of $^{99}\text{TcO}_4^-$ anions from low level radioactive aqueous waste was examined using batch technique. Different parameters affecting on the adsorption process were studied for the removal of $^{99}\text{TcO}_4^-$. The results revealed that NMO/AC (4 M, 6 M and 8 M) has a high adsorption efficiency (93.57%, 90.3% and 90.3%) respectively compared to NMO and AC which have a lower adsorption efficiency (41% and 38.9%) respectively. Moreover, the adsorption isotherm belonged to Freundlich model, the adsorption data followed pseudo-second order model and the thermodynamic study indicated that the adsorption of $^{99}\text{TcO}_4^-$ on Nano-composites was an exothermic and spontaneous process.

Keywords

Nano Manganese Oxide (NMO), Activated Carbon (AC), Technetium-99, Co-Precipitation, Adsorption

1. Introduction

Technetium-99 (^{99}Tc) is a pure β -emitter radionuclide with a half-life of 2.13×10^5 years. It is formed in the thermal neutron fission of ^{235}U with high yield (6%) [1] [2] and by spontaneous fission of ^{238}U in the earth's crust [3]. It also appears environmentally from the decay of the medical radioisotope $^{99\text{m}}\text{Tc}$ (6.0 h half-life) [4]. In uranium enrichment facilities, waste streams containing a high concentration of ^{99}Tc result from the decontamination of process equipment. Technetium-99 is very mobile in groundwater due to its existence dominantly as the anionic species, pertechnetate TcO_4^- [5]. The pertechnetate TcO_4^- is not immobilized by most common minerals or inorganic sorbents because it is repulsed by their negative charge [6].

A large amount of ^{99}Tc has been produced and released to the environment from nuclear installations, which makes ^{99}Tc the only environmentally significant Tc isotope. Meanwhile, ^{99}Tc can also be produced through neutron activation of ^{99}Mo . **Figure 1** shows the formation scheme of ^{99}Tc . The higher-water solubility of Tc (in the form of TcO_4^-), the longer half-life of ^{99}Tc , and thus long residence time in the oceans, make ^{99}Tc an ideal oceanographic tracer for investigation of movement, exchange and circulation of water masses. All these investigations and applications require an accurate determination of ^{99}Tc in various types of samples [7]. Technetium-99 is of particular concern to the U.S. Department of Energy (DOE), the Environmental Protection Agency (EPA), and the Nuclear Regulatory Commission (NRC) because of its persistence and mobility in the environment [8]. Technetium-99 is particularly mobile once released from the waste, since $^{99\text{m}}\text{Tc}$ is present in aqueous solutions in its stable heptavalent state as the pertechnetate anion, $^{99}\text{TcO}_4^-$. This oxo-anion is highly soluble in groundwater under oxidizing conditions and difficult to eliminate, posing concern as a significant environmental hazard [9].

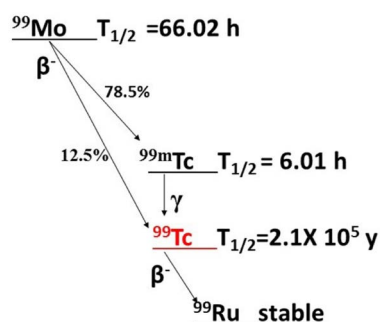


Figure 1. Decay scheme of ^{99}Mo .

Each nuclear facility generates about 40 kg of ^{99}Tc every year, most of which is disposed of as nuclear waste material [10]. ^{99}Tc has been widely distributed in the environment as a result of fallout from ballistics testing [11]. Activated carbon has been shown to retain pertechnetate ions efficiently [12] investigated the adsorption behavior of pertechnetate, $^{99\text{m}}\text{TcO}_4^-$ from various acid and salt concentrations. The mechanism behind the adsorption is not exactly known but ion-exchange with functional groups on the active carbon has been suggested by Gu *et al.*, in 1996 [13].

Nanoparticles have received an increasing amount of research interest. This is due to the unique size-dependent properties of nanoparticles, which are often thought as separate and intermediate state of the matter lying between individual atoms and bulk material [14]. Nanoparticles consisting of a large range of transition metals and metal oxides have found to exhibit advantageous size-dependent catalytic properties and are being investigated intensively [15] [16] [17] [18]. Nanomaterials [19] are having a length scale less than 100 nm which are having their potential applications of fascinating electrical, magnetic and catalytic properties [20].

In the present work, we applied the Co-precipitation method to synthesize MnO_2 nanoparticles (NMO) loaded with modified activated carbon after the treated with HNO_3 by different concentrations (4 M, 6 M and 8 M). The prepared composites are used as a low-cost adsorbent for the adsorption of Technetium-99 from aqueous solutions. The influence of various experimental parameters on $^{99}\text{TcO}_4^-$ adsorption process, in addition the optimum adsorption conditions were studied, sorption kinetics and the sorption capacity of NMO/ AC was evaluated using different isotherm models.

2. Materials and Methods

2.1. Chemicals and Reagents

All chemicals were analytical grade, purchased and used as received without further purification: Potassium Permanganate KMnO_4 ; Sigma-Aldrich, Manganese Chloride $\text{MnCl}_2 \cdot 4\text{H}_2\text{O}$; Merk, Activated Carbon (AC) commercial-grade provided by El-Gomhoria company for trade service (Cairo), ^{99}Tc radionuclide (activity 257.4 CPM/ml) was extracted from residual $^{99\text{m}}\text{Tc}$ columns from the technetium generator used in nuclear medicine centers, Ultima GoldTM (AB LSC-cocktail) from Packard bioscience company, concentrated acids of A.R HNO_3 , HCl and NaOH were used throughout the investigations as required and freshly bi-distilled water was used through all experiments.

2.2. Sorbent Preparation

A variety of sorbents were prepared for $^{99}\text{TcO}_4^-$ removal from the aqueous waste. Sorbent material includes 1) Nanosized manganese oxide (NMO) by co-precipitation method, at which the prepared 0.2 M KMnO_4 stirred with a magnetic stirrer, the pH was adjusted between pH 8 - 9 using 2 M NaOH then

dropwise 0.3 M MnCl₂. The suspension is stirred for 60 min then the precipitate is left overnight to settle. The solution is decanted to the extent possible, and the remaining suspension is centrifuged. The sample washed with bi-distilled water, dried under vacuum for two days and finally heated at 90°C till constant weight [21]. 2) Activated carbon (AC) was soaked overnight in three different HNO₃ concentrations (4 M, 6 M and 8 M) followed by heating at 80°C - 90°C for 6 hours with refluxing. The treated samples washed with bi-distilled water. The treated AC samples were dried under vacuum for two days and finally, heated at 900°C till constant weight, grinding and homogenized. 3) Mix the sorbents to evaluate the synergistic effects of modified activated carbon and NMO.

- The first composite prepared by mixed sorbent between NMO and modified activated carbon with 4 M HNO₃ with ratio (1:1) code (NMO/4 M AC).
- The second mixed sorbent between NMO and modified activated carbon with 6 M HNO₃ with ratio (1:1) code (NMO/6 M AC).
- The third mixed sorbent between NMO and modified activated carbon with 8 M HNO₃ with ratio (1:1) code (NMO/8 M AC).

These mixed sorbents were studied because of their low cost and expected high capacity to adsorb ⁹⁹TcO₄⁻ from low-level radioactive liquid waste.

2.3. Batch Sorption Experiment

The batch experiments were performed by 0.05 gm of sorbent which added to 5 ml of radioactive waste solutions into a polypropylene centrifuge tube. The suspensions were placed on a slow-moving shaker rotates at 200 rpm for 2 hours. Each suspension was passed through a 0.45 μm cellulose membrane filter with a diameter (25 mm). The effect of initial pH, contact time, initial concentration of adsorbate (⁹⁹Tc), ionic strength and temperature were investigated. The pH of the solution adjusted at the desired value by adding 0.1 M NaOH or HCl. The radionuclide concentrations of the filtrates were analyzed by a liquid scintillation counter (LSC) where 5 ml of the filtrate was added to 5 ml Packard Ultima Gold™ AB LSC-cocktail for effective beta discrimination LSC, for measuring the activity the LSC model Packard TRI CARB 2770 was used. The adsorption capacity of ⁹⁹Tc q_t (CPM/g) calculated by Equation (1).

Where: C_0 (CPM/L) is the initial concentration of ⁹⁹Tc, C_t (CPM/L) is the concentration of ⁹⁹Tc at time t , V (L) is the volume of ⁹⁹Tc solution, and m (g) the mass of sorbent.

$$q_t = (C_0 - C_t) \times \frac{V}{m} \quad (1)$$

The percent uptake or the removal efficiency ($R\%$) was calculated by Equation (2).

$$R\% = \frac{C_0 - C_t}{C_0} \times 100 \quad (2)$$

The equilibrium adsorption capacity of adsorbent, q_e (CPM/g) can be determined by Equation (3).

$$q_e = (C_0 - C_e) \times \frac{V}{m} \quad (3)$$

where: C_e (CPM/g) is the ^{99}Tc concentration at equilibrium in the supernatant after separation of the adsorbent and V , m , and C_0 have the same meaning as in Equations (1) & (2) [22].

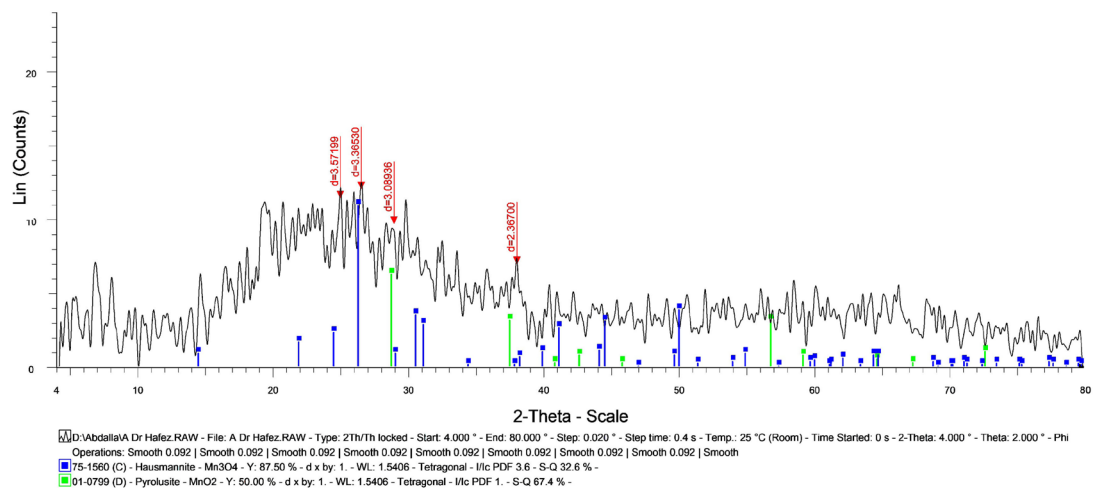
3. Results and Discussions

3.1. Structural Characterization

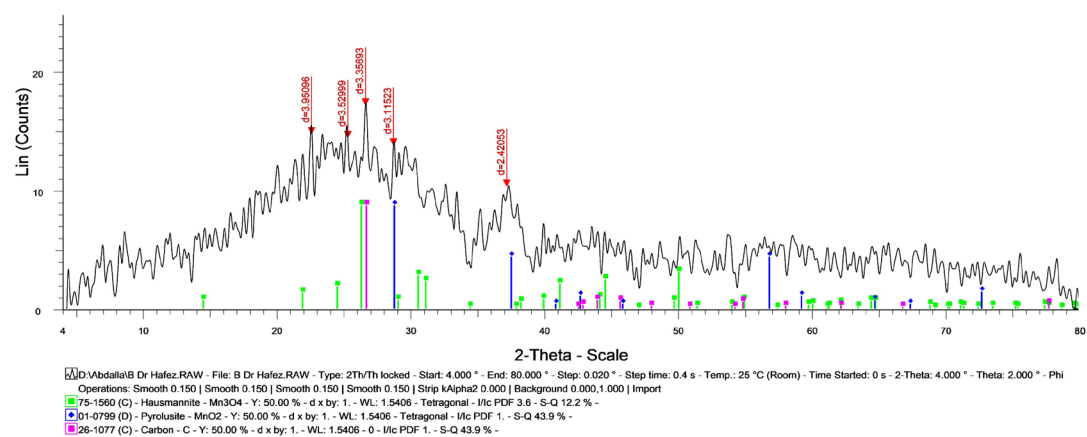
- X-Ray diffraction

X-ray diffraction (XRD) analysis was employed to study the phase composition of the synthesized composites, using a diffractometer (Bruker; D8 advance) with monochromator Cu-K α target wavelength 1.54178 Å, 40 kV, and 40 mA Germany.

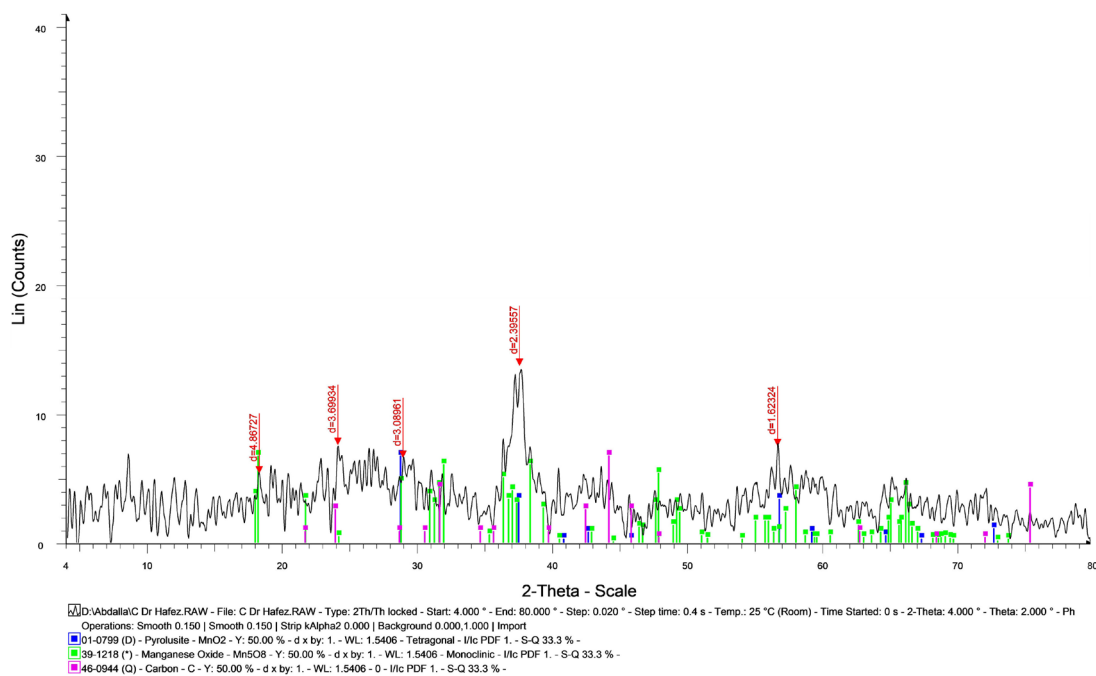
Figure 2 shows the XRD patterns of the produced NMO, NMO/(4 M, 6 M, 8 M) AC and AC. **Figure 2(a)** shows a broad diffraction pattern for NMO, which characteristic of pyrolusite tetragonal phase of $\beta\text{-MnO}_2$ at $2\theta = 28.877$ and $2\theta = 37.984$ indexed to (JCPDS 01-0799) [23] and hausmannite tetragonal phase of Mn_3O_4 at $2\theta = 24.907$ and $2\theta = 26.464$ related to (JCPDS 75-1560) [24] [25] meanwhile **Figure 2(b)** shows NMO/(4M AC) which fitted to pyrolusite tetragonal phase of $\beta\text{-MnO}_2$ at $2\theta = 26.531$ corresponding to (JCPDS 01-0799), hausmannite phase Mn_3O_4 at $2\theta = 22.485$, $2\theta = 25.209$ indexed to (JCPDS 75-1560) and carbon at $2\theta = 37.113$, $2\theta = 28.632$ related to (JCPDS 26-1077) [26] **Figure 2(c)** employed of NMO/(6M AC) the tetragonal crystalline phase pyrolusite $\beta\text{-MnO}_2$ at $2\theta = 28.875$ corresponding to (JCPDS 01-0799), monoclinic manganese oxide Mn_5O_8 at $2\theta = 18.212$, $2\theta = 56.659$ indexed to (JCPDS 39-1218) [27] and carbon at $2\theta = 37.514$ related to (JCPDS 46-0944) [28]. **Figure 2(d)** apply NMO/(8 M AC) presence of a diffraction peaks of pyrolusite tetragonal phase of $\beta\text{-MnO}_2$ at $2\theta = 29.11$ corresponding to (JCPDS 01-0799), manganese oxide monoclinic phase Mn_5O_8 at $2\theta = 17.824$, $2\theta = 58.064$ indexed to (JCPDS 39-1218), Ramsdellite orthorhombic phase $\gamma\text{-MnO}_2$ at $2\theta = 22.253$ (JCPDS 44-0142) [29] [30] and carbon at $2\theta = 37.594$ related to (JCPDS 26-1076) [31]. It was obvious that sharp diffraction beaks for carbon at $2\theta = 26.726$ indexed to (JCPDS 26-1077) in their diffraction patterns as depicted in **Figure 2(e)**. The subsequent phase transition into different valences of manganese oxide possibly owing to the oxidative atmosphere used at the beginning of the synthesis provides a pathway to oxidize some Mn^{2+} present in $\text{Mn}(\text{OH})_2$ to Mn^{3+} and Mn^{4+} during the drying step, the reducing reaction with these carbon matrix or the acidic treatment of carbon, then it seems that a partial amount of Mn^{3+} can be oxidized leading to Mn_5O_8 monoclinic phase, which stabilizes the divalent Mn ions inherited from Mn_3O_4 . Digestion time and acid concentration could explain this discrepancy [25] [32]. The calculated average crystallite size of the prepared NMO, NMO/(4 M AC), NMO/(6 M AC), NMO/(8 M AC) and AC are 11.6 nm, 16.9 nm, 9.6 nm, 14.3 nm and 21.4 nm respectively which calculated by Dedye-Scherer Equation (4) [33].



(a)



(b)



(c)

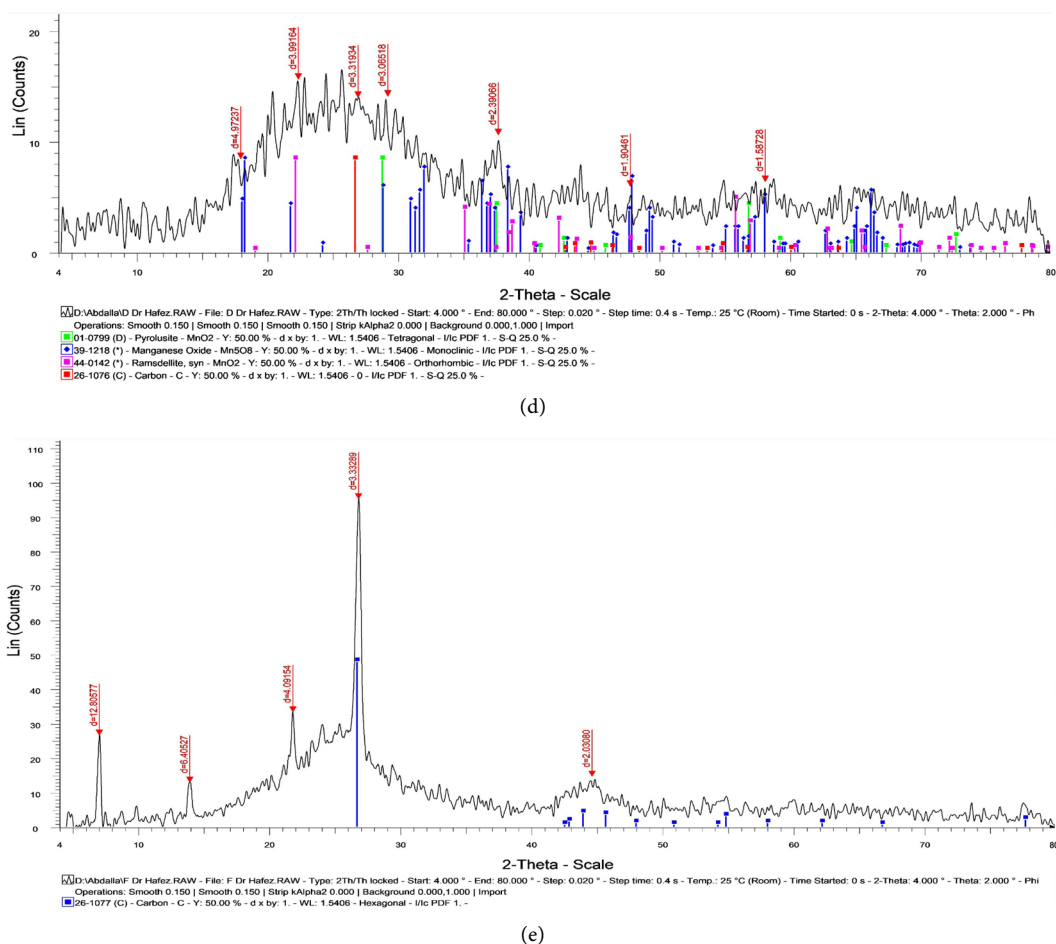


Figure 2. (a) XRD patterns of sample NMO; (b) XRD patterns of sample NMO/(4 M AC); (c) XRD patterns of sample NMO/(6 M AC); (d) XRD patterns of sample NMO/(8 M AC); (e) XRD patterns of sample AC.

$$D = \frac{0.9\lambda}{\beta \cos \theta_B} \quad (4)$$

where, λ (nm) is the X-ray radiation wavelength, β is the diffraction peak full width at half maximum (FWHM), and θ_B is the Bragg diffraction angle.

- FT-IR analysis

Fourier Transform Infra-Red spectroscopy (FTIR) model (BRUKER; VERTEX 70v) was used at room temperature in Egyptian Nuclear and Radiological Regulatory Authority for obtaining information about the functional groups in the structure. The FTIR spectra of samples NMO, NMO/(4M AC), NMO/(6M AC), NMO/(8M AC) and AC are depicted in **Figure 3** and the bands illustrated as follows. In 400 - 4000 cm^{-1} , the bands at 414 - 592 cm^{-1} should be ascribed to the Mn–O vibrations, and the bands at 750 - 1640 cm^{-1} are usually attributed to the –OH bending vibration with Mn atoms [34] [35], meanwhile, bands can be observed at 3400 - 3678 cm^{-1} which attributed to the O–H stretching vibration [36] [37]. The bands 1500 - 1900 cm^{-1} due to C = O stretching [37] [38], where the bands at 2846, 2912 cm^{-1} correspond to C–H symmetric and asymmetric respectively [37] [39]. It was found that bands at 3700 - 3899 cm^{-1}

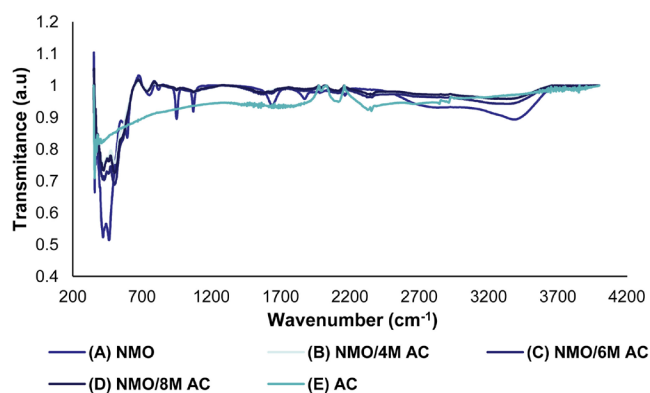


Figure 3. FT-IR spectra of (A) NMO; (B) NMO/4 M AC; (C) NMO/6 M AC; (D) NMO/8 M AC; (E) AC.

attributed to hydrogen bonds ($\text{H}_2\text{O}\dots\text{H}\dots\text{H}_2\text{O}$)⁺, which were formed between water and protons of acidic groups [40]. Finally, the wave number at bond 2356 cm^{-1} may be due to forming a new functional group $\text{NC} = \text{O}$ which can be turned into an electron structure [39].

3.2. Morphology Study

The Scanning Electron Microscope (SEM) with a microscope (JEOL JSM-6510LA) was used to study the surface morphology and the particle diameter of NMO, NMO/(4 M AC), NMO/(6 M AC), NMO/(8 M AC) and AC investigated by field emission. Figure 4 indicate the different morphology between the used adsorbents. Figure 4(a) showed that NMO is foamy, spongy and agglomerated. The size of agglomerates is about $50\text{ }\mu\text{m}$. Figure 4(b) show NMO/(4 M AC) like sea wave with void or pores and the agglomerates is $50\text{ }\mu\text{m}$. Figure 4(c) illustrate the morphology of NMO/(6 M AC) like aquatic plant, a narrow holes in wall with aggregates $50\text{ }\mu\text{m}$. Figure 4(d) for the composite NMO/(8 M AC) is composed of small single spheres, bulk agglomerates of sphere with average size $50\text{ }\mu\text{m}$. Figure 4(e) the SEM micrograph showed that the obtained nanoparticle has a flower, mushrooms and agglomerated, with an average size of agglomerates about $50\text{ }\mu\text{m}$.

3.3. Batch Adsorption Experiments

- Effect of solution pH

The pH of the solution is an important parameter that controlling the surface charge of the adsorbent and it has a significant change in the behavior of TcO_4^- ions. HNO_3 or HCl and NaOH were used to adjust the pH and reduction of Tc is favored at low pH and alkaline media oxidizes [41]. The results of the adsorbed pertechnetate TcO_4^- ion in pH range 2.3 to 7.04 shown in Figure 5.

It is observed that the percent uptake for the adsorbents NMO/(4 M, 6 M, 8 M) AC is higher than that of AC and NMO. The optimum pH value in case of using NMO/(4 M, 6 M, 8 M AC) as adsorbents is 2.33 whereas, in case AC alone and NMO are 3.02.

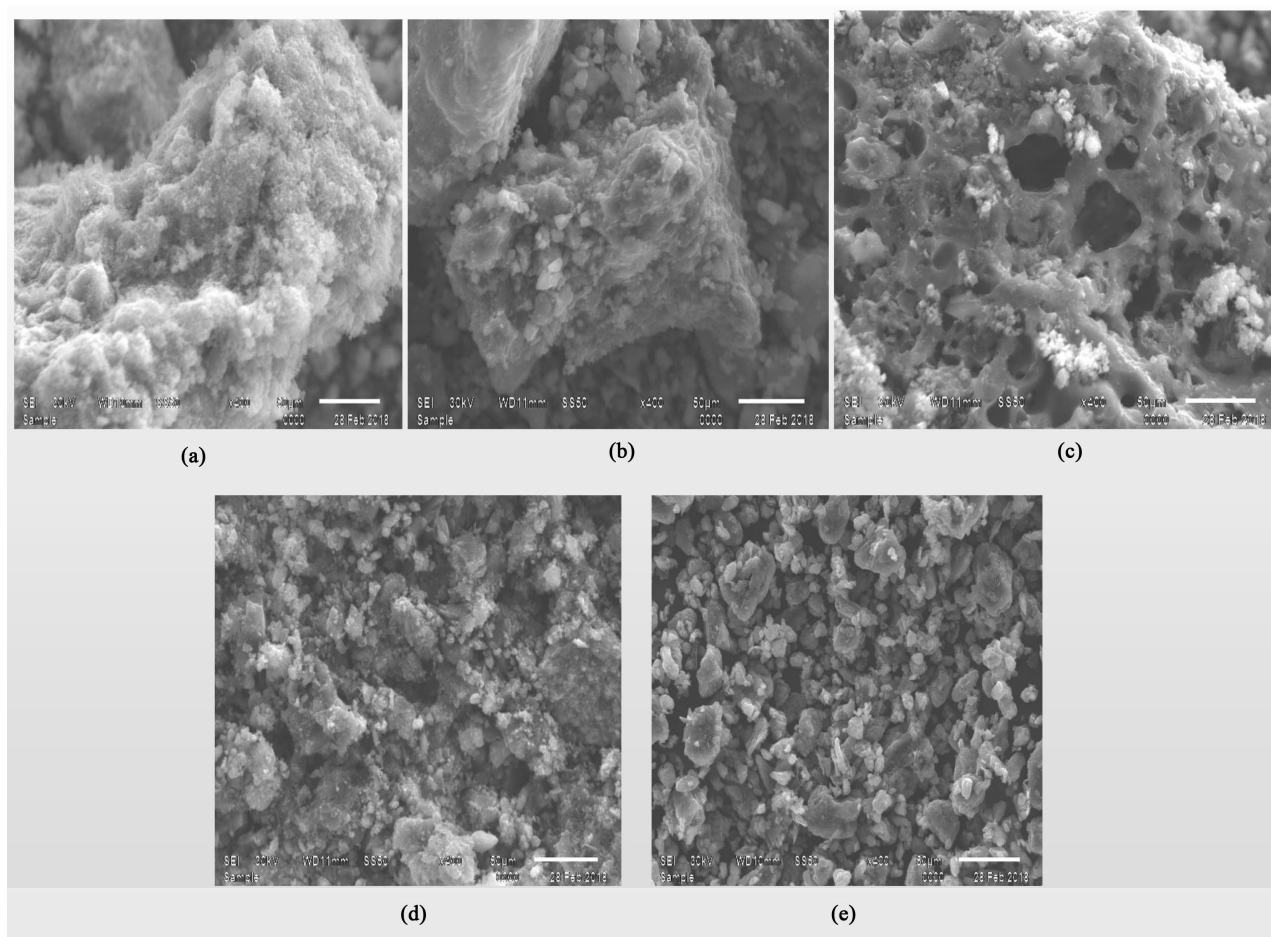


Figure 4. SEM images of samples (a) NMO; (b) NMO/4 M AC; (c) NMO/6 M AC; (d) NMO/8 M AC and (e) AC.

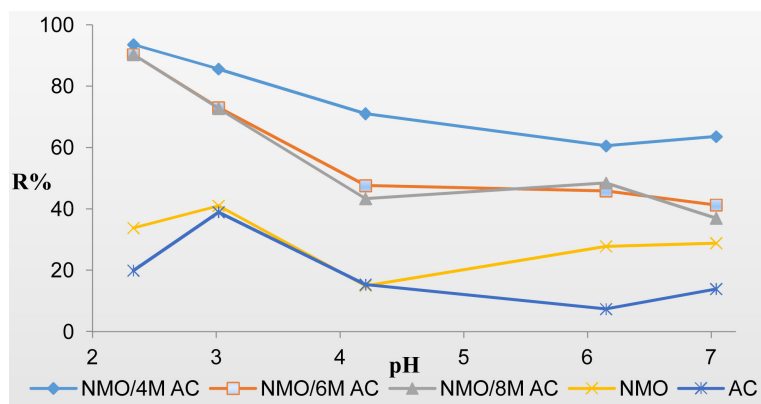


Figure 5. Effect of pH on TcO_4^- removal percent for samples NMO, NMO/(4 M AC), NMO/(6 M AC), NMO/(8 M AC) and AC.

The obtained maximum removal percentages for sorbents (NMO/4 M AC, NMO/6 M AC, NMO/8 M AC, NMO, AC) were 93.57%, 90.3%, 90.3%, 41%, 38.9% respectively.

It was found that the adsorption decreased as the pH increased from 2.33 to 7.04 for all the investigated samples **Figure 5**. This behavior could be explained

by the surface charge of the sorbent at lower pH values covered by protons (H^+) forming positively charged particles and the pertechnetate $^{99}TcO_4^-$ is negative which increases the electrostatic interaction between negative $^{99}TcO_4^-$ ions and the positive surface of the sorbents. While, at higher pH value there is a notable decrease in TcO_4^- removal this may be attributed to electrostatic repulsion between $^{99}TcO_4^-$ and the negatively charged surface of the sorbents. It is claimed that anion exchange sites ($AC^+ -NO_3^-$) were formed at pH value ~ 2 in nitrate solutions and at a higher pH value, there was a competition between pertechnetate ion and OH^- [12] [42].

- Effect of contact time

The influence of contact time on the adsorption efficiency of $^{99}TcO_4^-$ anions by a prepared composite were studied using 0.05 g of NMO/(4 M, 6 M, 8 M) AC at room temperature and initial activity concentration of 709 CPM/vial (141.8 CPM/ml) for $^{99}TcO_4^-$. The sorption of the investigated isotope $^{99}TcO_4^-$ increases with time to reach a saturation level for one-hour prolonged adsorption 24 hours did not a significant change of the equilibrium capacity for any of the investigated sorbents. **Figure 6** shows that there was no significant difference between the removal of $^{99}TcO_4^-$ by samples NMO/6 M AC and NMO/8 M AC whereas slight difference in the using NMO/4 M AC. Moreover, NMO and AC have lower efficient than the other composites.

The significant increase in the adsorption capacity for the anionic type of adsorbates could be attributed to the interaction of the Nano-manganese oxide loaded into the AC by 4 M, 6 M and 8 M [43]. This variation may be due to the initial large number of vacant sites on the adsorbent surface is available for adsorption and high gradient of solute concentration [44] [45]. The slow rate of adsorption may be due to decreasing in the number of vacant surface sites of adsorbent and remaining vacant surface sites are difficult to be occupied due to repulsive force between the solute molecules on the solid and bulk phases [46].

- Effect of temperature

The temperature of the reaction has a significant effect on the rate of the adsorption process. The adsorption process was carried out at different temperatures ($25^\circ C$, $30^\circ C$, $40^\circ C$ and $50^\circ C$) for $^{99}TcO_4^-$ ions using 0.05 gm of

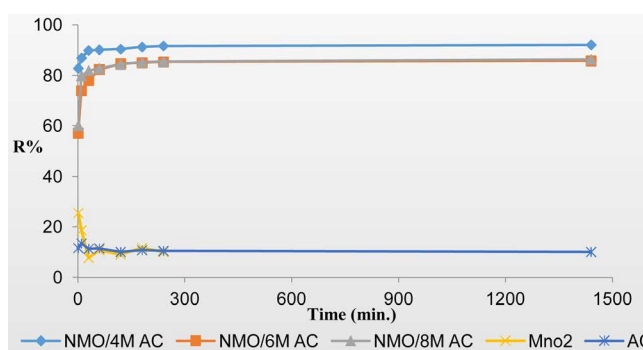


Figure 6. Effect of contact time on TcO_4^- removal percent by samples NMO, NMO/(4 M AC), NMO/(6 M AC), NMO/(8 M AC) and AC.

adsorbents (NMO/4 M AC, NMO/6 M AC and NMO/8 M AC), $^{99}\text{TcO}_4^-$ activity concentration 709 CPM/vial (5 ml) with stirring and contact time 60 min. **Figure 7** shows that the removal uptake decreased gradually with increasing the temperature of the solution which indicates the process may be exothermic reaction during the adsorption of $^{99}\text{TcO}_4^-$.

- **Effect of competing ion concentration**

The effect of competing ion concentration on the adsorption of $^{99}\text{TcO}_4^-$ on NMO/4 M AC, NMO/6 M AC, and NMO/8 M AC was studied by using KCl salt at a different concentration from 5 to 100 ppm. The result depicts in **Figure 8** illustrated that the solution ionic strength has a relatively very small effect on the removal percentage of $^{99}\text{TcO}_4^-$ ions.

- **Effect of initial $^{99}\text{TcO}_4^-$ activity concentration**

The adsorption process was carried out at a different initial concentration of $^{99}\text{TcO}_4^-$ at (102, 200, 368, 763 and 1287 CPM), pH 2.3 for 1 h contact time and at room temperature. From **Figure 9** the adsorption capacity increased with increasing the initial activity concentration of pertechnetate ions. The obtained results agree with other investigators Dowlen *et al.*, in 1996 [13]. The increase in the amount of adsorption was according to an increase in the electrostatic interaction between the pertechnetate ions and the adsorbent active sites due to the

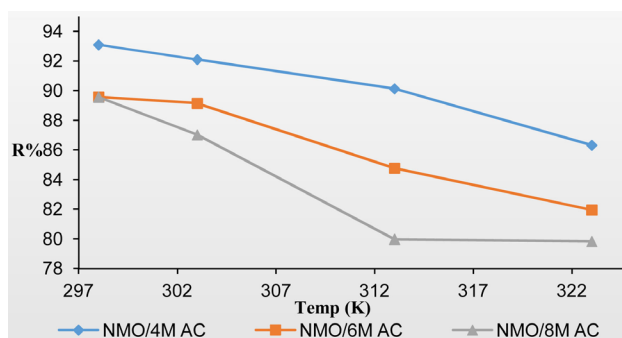


Figure 7. Effect of temperature on TcO_4^- removal percent by samples (NMO/4 M AC), (NMO/6 M AC) and (NMO/8 M AC).

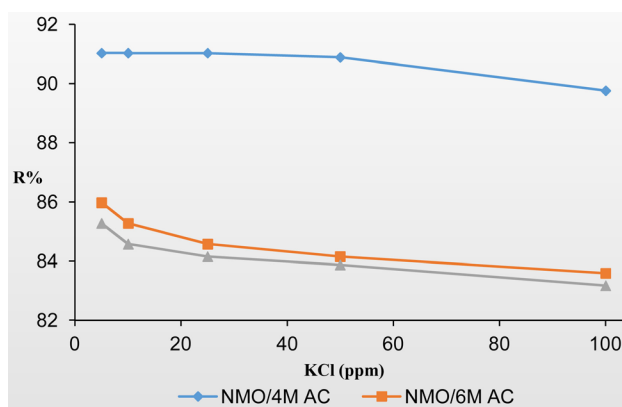


Figure 8. Effect of competing ion concentration on TcO_4^- removal percent by samples (NMO/4 M AC), (NMO/6 M AC) and (NMO/8 M AC).

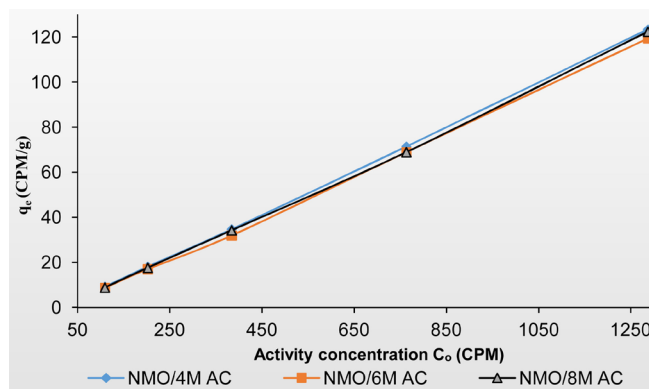


Figure 9. Effect of initial activity conc. of TcO_4^- on the adsorption capacity by samples (NMO/4 M AC), (NMO/6 M AC) and (NMO/8 M AC).

fact that more adsorption sites were being covered as the pertechnetate ions concentration increased [47].

3.4. Adsorption Isotherms

An adsorption isotherm is a curve describing the phenomenon governing the retention or mobility of a substance from the aqueous porous media or aquatic environments to a solid-phase at a constant temperature and pH [48] [49]. Adsorption equilibrium (the ratio between the adsorbed amount with the remaining in the solution) is established when an adsorbate containing phase has been contacted with the adsorbent for sufficient time, with its adsorbate concentration in the bulk solution is in a dynamic balance with the interface concentration [50] [51] was determined the adsorption capacity of $^{99}\text{TcO}_4^-$ onto NMO/4 M AC, NMO/6 M AC and NMO/8 M AC in the light of Langmuir and Freundlich adsorption isotherm models.

- *Langmuir isotherm model*

This empirical model assumes monolayer adsorption (the adsorbed layer is one molecule in thickness), adsorption can only occur at a finite (fixed) number of definite localized sites, that are identical and equivalent, with no lateral interaction and steric hindrance between the adsorbed molecules, even on adjacent sites [52]. In its derivation, Langmuir isotherm refers to homogeneous adsorption, in which each molecule possesses constant enthalpies and sorption activation energy (all sites possess an equal affinity for the adsorbate) [53], with no transmigration of the adsorbate in the plane of the surface [54]. Graphically, it is characterized by a plateau, an equilibrium saturation points where once a molecule occupies a site, no further adsorption can take place [49] [55]. The linear form of Langmuir isotherm equation is given as in Equation (5).

$$\frac{C_e}{q_e} = \frac{1}{Q_m \cdot K_L} + \frac{C_e}{Q_m} \quad (5)$$

where: C_e (CPM/L) is the equilibrium concentration of the adsorbate, q_e (CPM/g) is the amount of adsorbate adsorbed per unit mass of adsorbent, K_L

and Q_m are Langmuir constants and the adsorption capacity in (CPM/g) respectively. C_e/q_e is plotted against C_e , a straight line with slope $(1/Q_m)$ and intercept $(1/Q_m K_L)$ is obtained. The essential characteristics of Langmuir isotherm can be expressed by a dimensionless constant called separation factor or equilibrium parameter, R_L , defined by Weber and Chakkravorti Equation (6) [56].

$$R_L = \frac{1}{1 + K_L C_0} \quad (6)$$

Lower in R_L value reflects that adsorption is more favorable. In explanation, R_L value indicates the adsorption nature to be either unfavorable if ($R_L > 1$), linear ($R_L = 1$), favorable ($0 < R_L < 1$) or irreversible ($R_L = 0$). **Table 1** illustrates R_L values near to zero, which indicate irreversible adsorption process.

- Freundlich isotherm model

Freundlich isotherm model assumes that the adsorption takes place on a heterogeneous surface of the adsorbent and the linearized form of this model can be given by Equation (7) [57] [58].

$$\ln q_e = \ln K_F + \left(\frac{1}{n}\right) \ln C_e \quad (7)$$

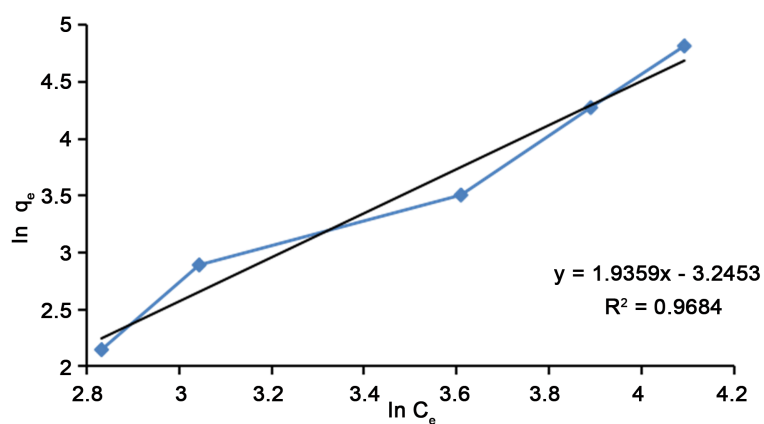
where: K_F is the Freundlich constant (CPM/g) which represents the relative adsorption capacity of the adsorbent. $(1/n)$ is the heterogeneity factor and it is a function of the strength of adsorption in the adsorption process and (n) has various values depending on the heterogeneity of the sorbent. if (n) lies between one and ten, this indicates a favorable sorption process [25]. $(1/n)$ and $\ln K_F$ values were calculated from the slope and intercept of the linear plots of $\ln q_e$ versus $\ln C_e$ which shows Freundlich isotherm as in **Figure 10** and **Table 1**.

The plot of $\ln q_e$ versus $\ln C_e$ gave a straight line with a slope of $(1/n)$ and intercept of $\ln K_F$ (Equation (7)). The slope ranges between 0 and 1 is a measure of adsorption intensity or surface heterogeneity, becoming more heterogeneous as its value gets closer to zero. Whereas, a value below unity implies chemisorption's process where $(1/n)$ above one is indicative of cooperative adsorption [59].

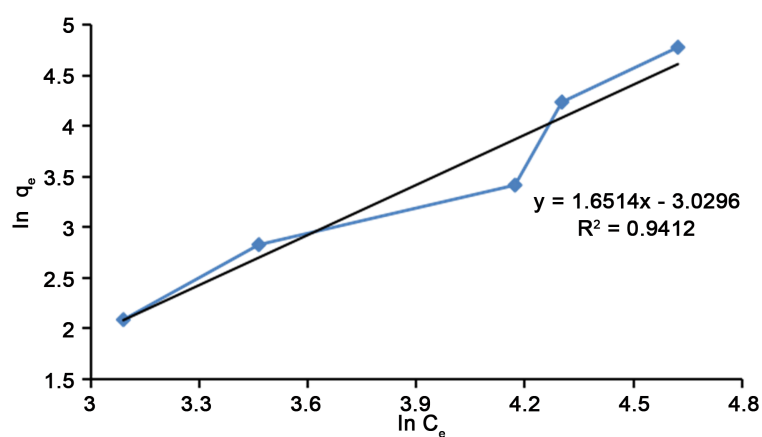
According to the results presented in **Table 1** the calculated correlation coefficients (R^2) for Freundlich Model were closer to unity so, this model may be the more appropriate than Langmuir Model. Moreover, the values of $(1/n)$ obtained

Table 1. Langmuir and Freundlich constants with R^2 values obtained for removal of $^{99}\text{TcO}_4^-$ by samples NMO/4 M AC, NMO/6 M AC and NMO/8 M AC.

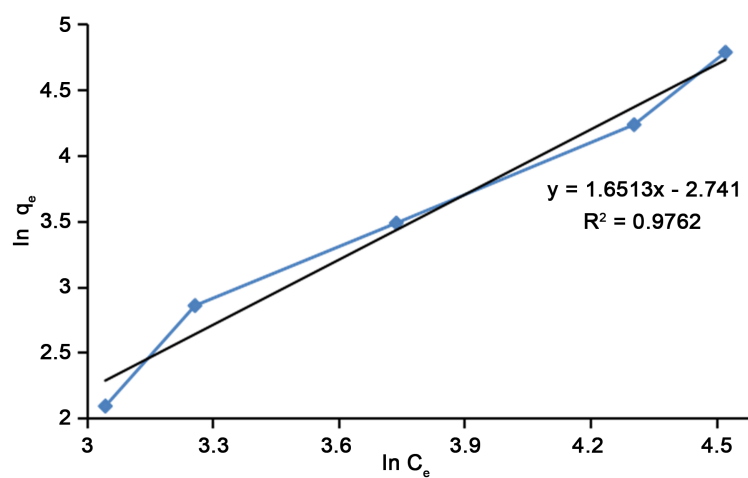
Adsorbent	Langmuir				Freundlich		
	$\frac{C_e}{q_e} = \frac{1}{Q_m \cdot K_L} + \frac{C_e}{Q_m}$				$\ln q_e = \ln K_F + \left(\frac{1}{n}\right) \ln C_e$		
	K_L	Q_m (CPM/g)	R_L	R^2	K_F	$1/n$	R^2
NMO/4 M AC	-0.013	-34.843	-0.062	0.807	0.039	1.935	0.988
NMO/6 M AC	-0.006	-48.309	-0.125	0.744	0.048	1.651	0.941
NMO/8 M AC	-0.007	-54.054	-0.111	0.671	0.065	1.651	0.976



(a)



(b)



(c)

Figure 10. Freundlich isotherm for (a) NMO/4 M AC; (b) NMO/6 M AC and (c) NMO/8 M AC.

from Freundlich Isotherm, equal 1.935, 1.6514 and 1.6513 for NMO/4 M AC, NMO/6 M AC and NMO/8 M AC respectively, $(1/n)$ above unity indicate bi-mechanism and cooperative adsorption [60].

Therefore, $^{99}\text{TcO}_4^-$ adsorption to NMO/4 M AC, NMO/6 M AC and NMO/8

M AC could be believed to be complex. The adsorption sites were most likely heterogeneous while the adsorption was not limited to be monolayer formation.

3.5. Kinetics Adsorption Models

To predict the adsorption kinetic model for adsorption $^{99}\text{TcO}_4^-$ from its radioactive liquid waste onto composites MnO_2/AC (4, 6, 8 M). The kinetics models: pseudo-first and second order models were applied to the experimental data. The best fit model was selected based on the linear regression correlation coefficient (R^2), which is a measure of how the predicted values from a forecast model match with the experimental data.

- Pseudo-first order model

It assumes that the rate of change of the solute uptake with time is directly proportional to the difference in the saturation concentration and the amount of solid uptake with the time, *i.e.* the rate of occupation sites is directly proportional to the number of unoccupied sites. Probably the earliest known and one of the most widely used kinetic equations so far for the adsorption of a solute from a liquid solution is the Lagergren equation or the pseudo-first order equation [61]. The pseudo-first order kinetics is calculated by Equation (8).

$$\log(q_e - q_t) = \log q_e - (K_1/2.303)t \quad (8)$$

where: K_1 is the rate constant of pseudo-first-order adsorption (min^{-1}), and q_e and q_t denote the amounts of adsorbed $^{99}\text{TcO}_4^-$ anions at equilibrium and at time t ($\text{Bq}\cdot\text{g}^{-1}$) respectively. Plot of $\log(q_e - q_t)$ versus t should give a straight line to confirm the applicability of the kinetic model, $\log q_e$ should be equal to the intercept and K_1 the slope as disputed in Figure 11 and Table 2.

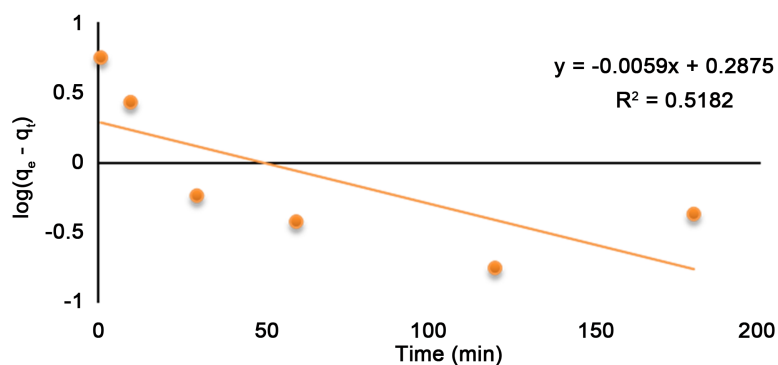
- Pseudo-second order model

It assumes that the rate of occupation of adsorption sites is proportional to the square of the number of unoccupied sites. Where the rate limiting step may be chemical sorption involving valence forces through sharing or exchange of electrons between TcO_4^- and sorbent [62]. The pseudo-second order equation is applied in the given form Equation (9).

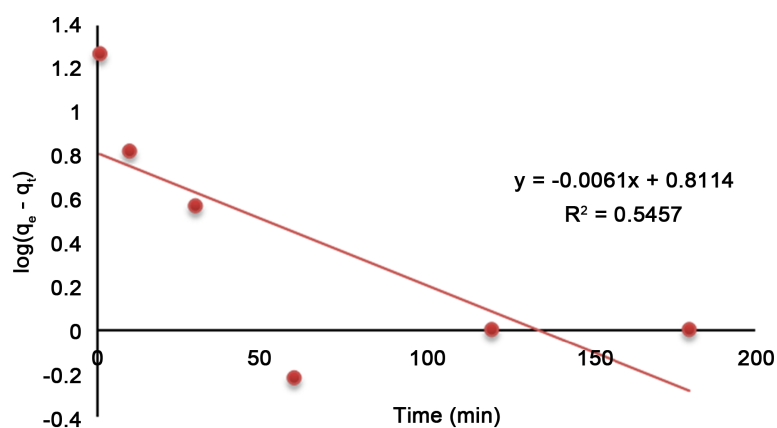
$$t/q_t = 1/(k_2 q_e^2) + (1/q_e)t \quad (9)$$

Table 2. Pseudo-first and second orders coefficients of sorption kinetics for $^{99}\text{TcO}_4^-$ removal by NMO/4 M AC, NMO/6 M AC and NMO/8 M AC and their correlations R^2 .

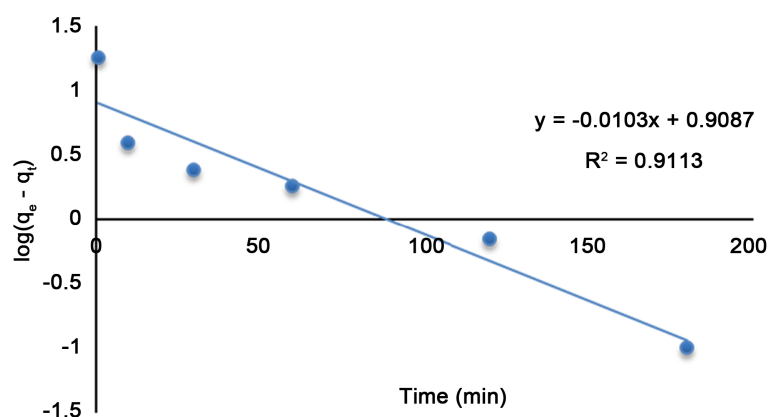
Adsorbent	pseudo-first order				pseudo-second order			
	$\log(q_e - q_t) = \log q_e - (K_1/2.303)t$				$t/q_t = 1/(k_2 q_e^2) + (1/q_e)t$			
	K_1	$q_e(\text{cal})$	$q_e(\text{exp})$	R^2	K_2	$q_e(\text{cal})$	$q_e(\text{exp})$	R^2
NMO/4 M AC	0.020	64.275	3.837	0.518	0.013	64.275	65.359	1
NMO/6 M AC	0.028	60.40	13.035	0.545	0.0152	60.40	60.975	1
NMO/8 M AC	0.024	60.50	8.104	0.911	0.0150	60.50	61.349	1



(a)



(b)



(c)

Figure 11. Pseudo-first order for samples (a) NMO/4 M AC; (b) NMO/6 M AC and (c) NMO/8 M AC.

where: k_2 ($\text{CPM} \cdot \text{g}^{-1} \cdot \text{min}^{-1}$) is the rate constant of the pseudo-second order adsorption. Additionally, the initial adsorption rate h ($\text{CPM} \cdot \text{g}^{-1} \cdot \text{min}^{-1}$) can be determined using Equation (10) [63].

$$h = K_2 \cdot q_e^2 \quad (10)$$

Plot of t/q_t versus t should give a straight line, $1/q_e$ equal the intercept and $1/K_2 q_e^2$ the slope as shown in **Figure 12**. **Table 2** illustrate the value of the

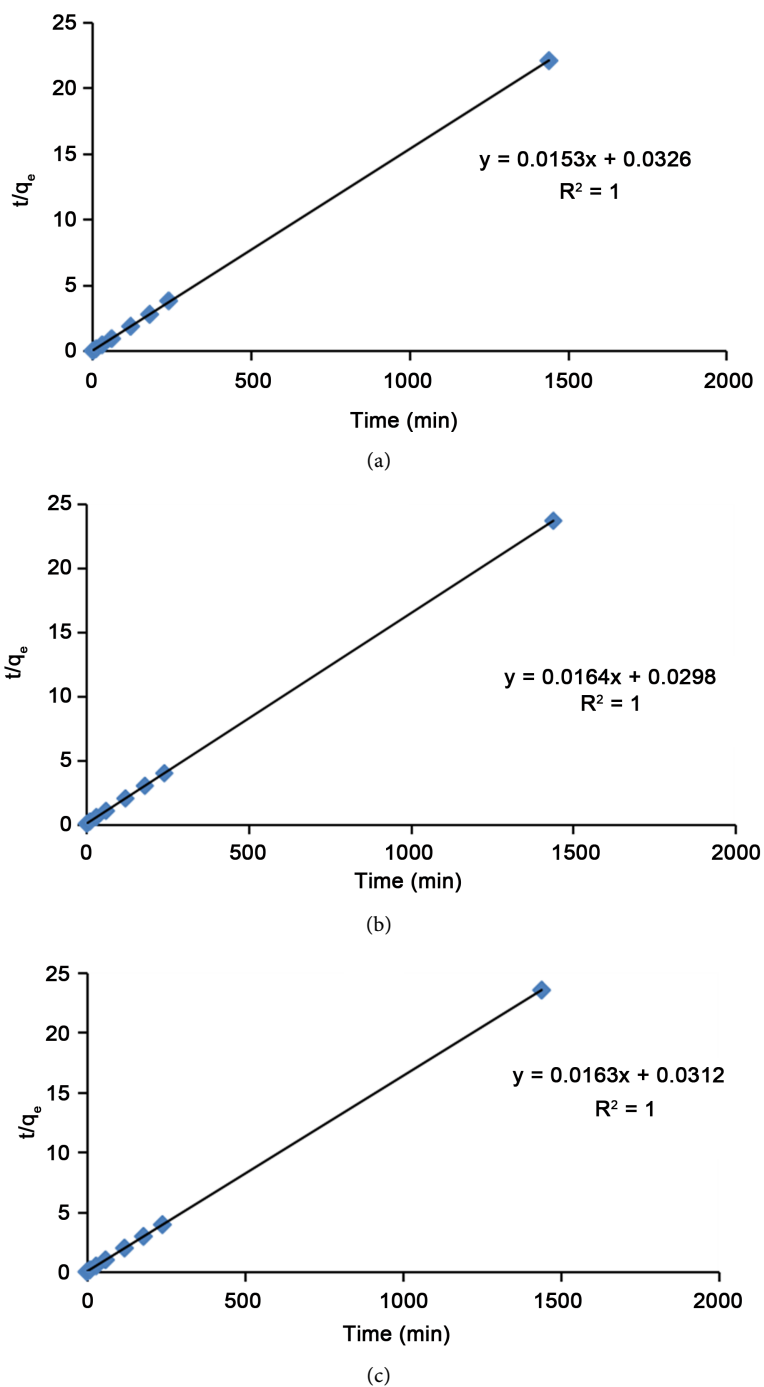


Figure 12. Pseudo-second order for samples (a) NMO/4 M AC; (b) NMO/6 M AC and (c) NMO/8 M AC.

correlation coefficient (R^2) is unity comparing with that obtained from the pseudo-first order. Moreover, the value of the calculated equilibrium adsorption capacity $q_e(\text{Cal})$ according to the pseudo-second order model is much closer to the experimentally obtained $q_e(\text{exp})$ on comparing to the calculated from the pseudo-first order model. It could be stated that the adsorption of $^{99}\text{TcO}_4^-$ onto NMO/4 M AC, NMO/6 M AC and NMO/8 M AC obeyed the pseudo-second

order kinetics model.

3.6. Adsorption Thermodynamic

The concept of thermodynamic assumes that in an isolated system where the energy cannot be gained or lost, the entropy change is the driving force [64].

Van't hoff Equation (11) was used to calculate the thermodynamic parameters such as change in enthalpy (ΔH°), a change in entropy (ΔS°) and change in Gibbs free energy (ΔG°). Adsorption of $^{99}\text{TcO}_4^-$ on the investigated materials, at different temperatures was determined by using Equations (12) & (13) and illustrated in **Figure 13**.

$$\ln K_d = \frac{\Delta S^\circ}{R} - \frac{\Delta H^\circ}{RT} \quad (11)$$

where: R (8.314 J/mol K) is the universal gas constant, T (K) the absolute solution temperature and K_d is the equilibrium constant which can be calculated as:

$$K_d = \frac{C_{Ae}}{C_e} \quad (12)$$

C_{Ae} (CPM/L) is the activity concentration of $^{99}\text{TcO}_4^-$ adsorbed on solid at equilibrium and C_e (CPM/L) is the equilibrium concentration of $^{99}\text{TcO}_4^-$ in the solution. The values of ΔH° and ΔS° were calculated from the slope and intercept of plot between $\ln K_d$ versus $1/T$ **Figure 13**. ΔG° can be calculated using the Equation (13) [65] [66]:

$$\Delta G^\circ = \Delta H^\circ - T\Delta S^\circ \quad (13)$$

The obtained values of thermodynamic parameters, (ΔH° , ΔS° and ΔG°), are presented in **Table 3**, the negative value of ΔH° indicates the exothermic nature of Nanosized MnO_2/AC (4 M, 6 M & 8 M). The negative value of ΔG° confirmed the feasibility of the process and the spontaneous nature of the sorption with a high preference for $^{99}\text{TcO}_4^-$.

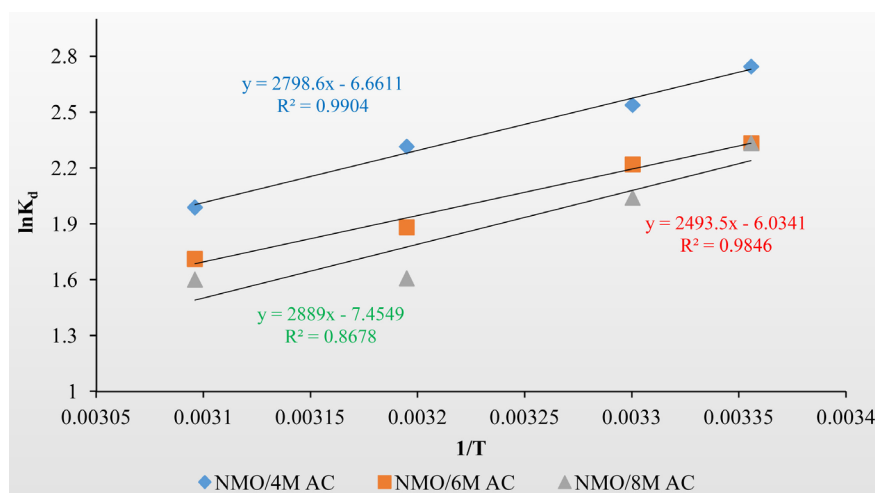


Figure 13. Van't Hoff plot for adsorption of $^{99}\text{TcO}_4^-$ on NMO/4 M AC, NMO/6 M AC and NMO/8 M AC.

Table 3. ΔH° , ΔG° and ΔS° obtained for removal $^{99}\text{TcO}_4^-$ on NMO/4 M AC, NMO/6 M AC and NMO/8 M AC.

Adsorbent	ΔH° (kJ/mol)	ΔS° (J/mol·K)	ΔG° (kJ/mol)			
			298 K	303 K	313 K	323 K
NMO/4 M AC	-23.267	-55.380	-6.764	-6.487	-5.933	-5.379
NMO/6 M AC	-20.731	-50.167	-5.781	-5.530	-5.028	-4.526
NMO/8 M AC	-24.019	-61.980	-5.549	-5.239	-4.619	-3.999

4. Conclusion

Low-cost adsorbents NMO, NMO/4 M AC, NMO/6 M AC and NMO/8 M AC have been prepared successfully and examined for their ability for removal of $^{99}\text{TcO}_4^-$ anions from low level radioactive liquid waste. The influence of major parameters governing the efficiency of the process such as, solution pH, competing ion concentration, initial activity concentration, and contact time on the removal process was investigated. The removal efficiency of $^{99}\text{TcO}_4^-$ reached 93.57%, 90.3% and 90.3% for the adsorbents NMO/4 M AC, NMO/6 M AC and NMO/8M AC respectively at contact time about 60 min. The kinetic study showed the rate of the reaction is Pseudo second order and the adsorption isotherm showed that the reaction followed Freundlich isotherm model, which describes chemisorption between NMO/(4M, 6 M, 8 M) AC and $^{99}\text{TcO}_4^-$ with a heterogeneous surface of the adsorbent. The adsorption thermodynamics showed negative values of free energy (ΔG°) and enthalpy (ΔH°) which indicates that the adsorption of $^{99}\text{TcO}_4^-$ anions on NMO/(4 M, 6 M, 8 M) AC is a spontaneous process and exothermic in nature of the reaction. Finally, it may be concluded that composites NMO/(4 M, 6 M, 8 M) AC are efficient sorbents for removal of $^{99}\text{TcO}_4^-$ from low level radioactive liquid waste.

Conflicts of Interest

The authors declare no conflicts of interest regarding the publication of this paper.

References

- [1] Liang, L., Gu, B. and Yin, X. (1996) Removal of Technetium-99 from Contaminated Groundwater with Sorbents and Reductive Materials. *Separations Technology*, **6**, 111-122. [https://doi.org/10.1016/0956-9618\(96\)00148-8](https://doi.org/10.1016/0956-9618(96)00148-8)
- [2] Li, D., Kaplan, D.I., Knox, A.S., Crapse, K.P. and Diprete, D.P. (2014) Aqueous ^{99}Tc , ^{129}I and ^{137}Cs Removal from Contaminated Groundwater and Sediments Using Highly Effective Low-Cost Sorbents. *Journal of Environmental Radioactivity*, **136**, 56-63. <https://doi.org/10.1016/j.jenvrad.2014.05.010>
- [3] CSchwochau, K. (1983) The Present Status of Technetium Chemistry. *Radiochimica Acta*, **32**, 139-152. <https://doi.org/10.1524/ract.1983.32.13.139>
- [4] Larsen, I.L., Stetar, E.A. and Glass, K.D. (1995) In-House Screening for Radioactive Sludge at A Municipal Wastewater Treatment Plant. *Radiation Protection Manager*,

12, 29.

- [5] Icenhower, J.P., Qafoku, N.P., Zachara, J.M. and Martin, W.J. (2010) The Biogeochemistry of Technetium: A Review of the Behavior of an Artificial Element in the Natural Environment. *American Journal of Science*, **310**, 721-752. <https://doi.org/10.2475/08.2010.02>
- [6] Abdellah, W.M., Ezzat, A. and Samir, I. (2019) Removal of Per technetate ($^{99}\text{TcO}_4^-$) from Liquid Waste by Magnesium Ferrite (MgFe_2O_4) Nanoparticles Synthesized Using Sol-Gel Auto Combustion Method. *Open Journal of Applied Sciences*, **9**, 968-986.
- [7] Shi, K., Hou, X., Roos, P. and Wu, W. (2012) Determination of Technetium-99 in Environmental Samples: A Review. *Analytica Chimica Acta*, **709**, 1-20. <https://doi.org/10.1016/j.aca.2011.10.020>
- [8] Mattus, A.J., Gilliam, T.M. and Dole, L.R. (1988) Review of EPA, DOE, and NRC Regulations on Establishing Solid Waste Performance Criteria. ORNL/TM-9322. Oak Ridge National Lab, TN (USA). <https://doi.org/10.2172/6963288>
- [9] Bishop, M.E., Dong, H., Kukkadapu, R.K., Liu, C. and Edelman, R.E. (2011) Bio-reduction of Fe-Bearing Clay Minerals and Their Reactivity toward Per technetate (Tc-99). *Geochimica et Cosmochimica Acta*, **75**, 5229-5246. <https://doi.org/10.1016/j.gca.2011.06.034>
- [10] Lieser, K.H. (1993) Technetium in the Nuclear Fuel Cycle, in Medicine and in the Environment. *Radiochimica Acta*, **63**, 5-8. <https://doi.org/10.1524/ract.1993.63.special-issue.5>
- [11] García-León, M., Manjón, G. and Sanchez-Angulo, C.I. (1993) $^{99}\text{Tc}/^{137}\text{Cs}$ Activity Ratios in Rainwater Samples Collected in the South of Spain. *Journal of Environmental Radioactivity*, **20**, 49-61. [https://doi.org/10.1016/0265-931X\(93\)90018-3](https://doi.org/10.1016/0265-931X(93)90018-3)
- [12] Yamagishi, I. and Kubota, M. (1989) Separation of Technetium with Active Carbon. *Journal of Nuclear Science and Technology*, **26**, 60-66. <https://doi.org/10.1080/18811248.1989.9734424>
- [13] Gu, B., Dowlen, K.E., Liang, L. and Clausen, J.L. (1996) Efficient Separation and Recovery of Technetium-99 from Contaminated Groundwater. *Separations Technology*, **6**, 123-132. [https://doi.org/10.1016/0956-9618\(96\)00147-6](https://doi.org/10.1016/0956-9618(96)00147-6)
- [14] Kormann, H.P., Schmid, G., Pelzer, K., Philippot, K. and Chaudret, B. (2004) Gas phase Catalysis by Metal Nanoparticles in Nanoporous Alumina Membranes. *Zeitschrift für anorganische und allgemeine Chemie*, **630**, 1913-1918. <https://doi.org/10.1002/zaac.200400192>
- [15] Stowell, C.A. and Korgel, B.A. (2005) Iridium Nanocrystal Synthesis and Surface Coating-Dependent Catalytic Activity. *Nano Letters*, **5**, 1203-1207. <https://doi.org/10.1021/nl050648f>
- [16] Subramanian, V., Wolf, E.E. and Kamat, P.V. (2004) Catalysis with TiO_2 /Gold Nanocomposites. Effect of Metal Particle Size on the Fermi Level Equilibration. *Journal of the American Chemical Society*, **126**, 4943-4950. <https://doi.org/10.1021/ja0315199>
- [17] Frank, M. and Bäumer, M. (2000) From Atoms to Crystallites: Adsorption on Oxide-Supported Metal Particles. *Physical Chemistry Chemical Physics*, **2**, 3723-3737. <https://doi.org/10.1039/b004091f>
- [18] Somorjai, G.A. (1997) New Model Catalysts (Platinum Nanoparticles) and New Techniques (SFG and STM) for Studies of Reaction Intermediates and Surface Restructuring at High Pressures during Catalytic Reactions. *Applied Surface Science*,

- 121, 1-19. [https://doi.org/10.1016/S0169-4332\(97\)00255-9](https://doi.org/10.1016/S0169-4332(97)00255-9)
- [19] Kudesia, V. (1997) Environmental Chemistry. Pragati prakashan, Meerut.
- [20] Lee, H.Y. and Goodenough, J.B. (1999) Supercapacitor Behavior with KCl Electrolyte. *Journal of Solid-State Chemistry*, **144**, 220-223. <https://doi.org/10.1006/jssc.1998.8128>
- [21] Nour, S., El-Sharkawy, A., Burnett, W.C. and Horwitz, E.P. (2004) Radium-228 Determination of Natural Waters via Concentration on Manganese Dioxide and Separation Using Diphonix Ion Exchange Resin. *Applied Radiation and Isotopes*, **61**, 1173-1178. <https://doi.org/10.1016/j.apradiso.2004.04.001>
- [22] Vijayakumar, G., Tamilarasan, R. and Dharmendirakumar, M. (2012) Adsorption, Kinetic, Equilibrium and Thermodynamic Studies on the Removal of Basic Dye Rhodamine-B from Aqueous Solution by the Use of Natural Adsorbent Perlite. *Journal of Materials and Environmental Science*, **3**, 157-170.
- [23] Zhu, S., Zhang, D., Li, Z., Furukawa, H. and Chen, Z. (2008) Precision Replication of Hierarchical Biological Structures by Metal Oxides Using a Sonochemical Method. *Langmuir*, **24**, 6292-6299. <https://doi.org/10.1021/la7037153>
- [24] Xiao, F. and Xu, Y. (2012) Pulse Electrodeposition of Manganese Oxide for High-Rate Capability Supercapacitors. *International Journal of Electrochemical Science*, **7**, 7440-7450.
- [25] Pang, H., Yang, Z., Lv, J., Yan, W. and Guo, T. (2014) Novel MnO_x at Carbon Hybrid Nanowires with Core/Shell Architecture as Highly Reversible Anode Materials for Lithium Ion Batteries. *Energy*, **69**, 392-398. <https://doi.org/10.1016/j.energy.2014.03.029>
- [26] Guo, C., Liu, Y., Ma, X., Qian, Y. and Xu, L. (2006) Synthesis of Tungsten Carbide Nanocrystal via a Simple Reductive Reaction. *Chemistry Letters*, **35**, 1210-1211. <https://doi.org/10.1246/cl.2006.1210>
- [27] Aghazadeh, M., Ghannadi Maragheh, M., Ganjali, M.R. and Norouzi, P. (2017) Preparation and Characterization of Mn₅O₈ Nanoparticles: A Novel and Facile Pulse Cathodic Electrodeposition Followed by Heat Treatment. *Inorganic and Nano-Metal Chemistry*, **47**, 1085-1089. <https://doi.org/10.1080/24701556.2017.1284092>
- [28] Yi, J., Qing, Y., Wu, C., Zeng, Y., Wu, Y., Lu, X. and Tong, Y. (2017) Lignocellulose-Derived Porous Phosphorus-Doped Carbon as Advanced Electrode for Supercapacitors. *Journal of Power Sources*, **351**, 130-137. <https://doi.org/10.1016/j.jpowsour.2017.03.036>
- [29] Tizfahm, J., Aghazadeh, M., Maragheh, M.G., Ganjali, M.R., Norouzi, P. and Faridbod, F. (2016) Electrochemical Preparation and Evaluation of the Supercapacitive Performance of MnO₂ Nano-Worms. *Materials Letters*, **167**, 153-156. <https://doi.org/10.1016/j.matlet.2015.12.158>
- [30] Ryu, W.H., Eom, J.Y., Yin, R.Z., Han, D.W., Kim, W.K. and Kwon, H.S. (2011) Synergistic Effects of Various Morphologies and Al Doping of Spinel LiMn₂O₄ Nanostructures on the Electrochemical Performance of Lithium-Rechargeable Batteries. *Journal of Materials Chemistry*, **21**, 15337-15342. <https://doi.org/10.1039/c1jm10146c>
- [31] Cahen, S., Furdin, G., Marêche, J.F. and Albiniaik, A. (2008) Synthesis and Characterization of Carbon-Supported Nanoparticles for Catalytic Applications. *Carbon*, **46**, 511-517. <https://doi.org/10.1016/j.carbon.2007.12.017>
- [32] Torres, J.Q., Giraudon, J.M. and Lamonier, J.F. (2011) Formaldehyde Total Oxidation over Mesoporous MnO_x Catalysts. *Catalysis Today*, **176**, 277-280.

<https://doi.org/10.1016/j.cattod.2010.11.089>

- [33] Jenkins, R. and Snyder, R.L. (1996) Introduction to X-Ray Powder Diffractometry (No. 543.427 JEN). <https://doi.org/10.1002/9781118520994>
- [34] Aghazadeh, M., Asadi, M., Maragheh, M.G., Ganjali, M.R., Norouzi, P. and Faridbod, F. (2016) Facile Preparation of MnO₂ Nanorods and Evaluation of Their Supercapacitive Characteristics. *Applied Surface Science*, **364**, 726-731. <https://doi.org/10.1016/j.apsusc.2015.12.227>
- [35] Aghazadeh, M., Maragheh, M.G., Ganjali, M.R., Norouzi, P. and Faridbod, F. (2016) Electrochemical Preparation of MnO₂ Nanobelts through Pulse Base-Electrogeneration and Evaluation of Their Electrochemical Performance. *Applied Surface Science*, **364**, 141-147. <https://doi.org/10.1016/j.apsusc.2015.12.146>
- [36] Luo, C., Wei, R., Guo, D., Zhang, S. and Yan, S. (2013) Adsorption Behavior of MnO₂ Functionalized Multi-Walled Carbon Nanotubes for the Removal of Cadmium from Aqueous Solutions. *Chemical Engineering Journal*, **225**, 406-415. <https://doi.org/10.1016/j.cej.2013.03.128>
- [37] Petrović, Đ., Đukić, A., Kumrić, K., Babić, B., Momčilović, M., Ivanović, N. and Matović, L. (2014) Mechanism of Sorption of Perchnetate onto Ordered Mesoporous Carbon. *Journal of Radioanalytical and Nuclear Chemistry*, **302**, 217-224. <https://doi.org/10.1007/s10967-014-3249-0>
- [38] Sivakumar, B., Kannan, C. and Karthikeyan, S. (2012) Preparation and Characterization of Activated Carbon Prepared from *Balsamodendron caudatum* Wood Waste through Various Activation Processes. *Rasayan Journal of Chemistry*, **5**, 321-327.
- [39] Rudyardjo, D.I. and Wijayanto, S. (2017) The Synthesis and Characterization of Hydrogel Chitosan-Alginate with the Addition of Plasticizer Lauric Acid for Wound Dressing Application. *Journal of Physics: Conference Series*, **853**, Article ID: 012042. <https://doi.org/10.1088/1742-6596/853/1/012042>
- [40] Gomez-Serrano, V., Pastor-Villegas, J., Perez-Florindo, A., Duran-Valle, C. and Valenzuela-Calahorra, C. (1996) FT-IR Study of Rockrose and of Char and Activated Carbon. *Journal of Analytical and Applied Pyrolysis*, **36**, 71-80. [https://doi.org/10.1016/0165-2370\(95\)00921-3](https://doi.org/10.1016/0165-2370(95)00921-3)
- [41] Holm, E., Gäfvert, T., Lindahl, P. and Roos, P. (2000) *In Situ* Sorption of Technetium Using Activated Carbon. *Applied Radiation and Isotopes*, **53**, 153-157. [https://doi.org/10.1016/S0969-8043\(00\)00127-5](https://doi.org/10.1016/S0969-8043(00)00127-5)
- [42] Ito, K. and Akiba, K. (1991) Adsorption of Perchnetate Ion on Active Carbon from Acids and Their Salt Solutions. *Journal of Radioanalytical and Nuclear Chemistry*, **152**, 381-390. <https://doi.org/10.1007/BF02104691>
- [43] Ma, J., Cui, B., Dai, J. and Li, D. (2011) Mechanism of Adsorption of Anionic Dye from Aqueous Solutions onto Organobentonite. *Journal of Hazardous Materials*, **186**, 1758-1765. <https://doi.org/10.1016/j.jhazmat.2010.12.073>
- [44] Naima, A., Mohamed, B., Hassiba, M. and Zahra, S. (2013) Adsorption of Lead from Aqueous Solution onto Untreated Orange Barks. *Chemical Engineering Transactions*, **32**, 55-60.
- [45] Hemmati, F., Norouzbeigi, R., Sarbisheh, F. and Shayesteh, H. (2016) Malachite Green Removal Using Modified Sphagnum Peat Moss as a Low-Cost Biosorbent: Kinetic, Equilibrium and Thermodynamic Studies. *Journal of the Taiwan Institute of Chemical Engineers*, **58**, 482-489. <https://doi.org/10.1016/j.jtice.2015.07.004>
- [46] Liyaghati-Delshad, M. and Moradi, R. (2014) Removal of Sr²⁺ from Aqueous Solutions by Adsorbent Activated Carbon of Almond Shell. *International Researcher*

Journal Applications Basic Sciences, **8**, 1950-1958.

- [47] Larous, S., Meniai, A.H. and Lehocine, M.B. (2005) Experimental Study of the Removal of Copper from Aqueous Solutions by Adsorption Using Sawdust. *Desalination*, **185**, 483-490. <https://doi.org/10.1016/j.desal.2005.03.090>
- [48] Ho, Y.S. (2006) Second-Order Kinetic Model for the Sorption of Cadmium onto Tree Fern: A Comparison of Linear and Non-Linear Methods. *Water Research*, **40**, 119-125. <https://doi.org/10.1016/j.watres.2005.10.040>
- [49] Limousin, G., Gaudet, J.P., Charlet, L., Szenknect, S., Barthes, V. and Krimissa, M. (2007) Sorption Isotherms: A Review on Physical Bases, Modeling and Measurement. *Applied Geochemistry*, **22**, 249-275. <https://doi.org/10.1016/j.apgeochem.2006.09.010>
- [50] Kumar, K.V. and Sivanesan, S. (2007) Sorption Isotherm for Safranin onto Rice Husk: Comparison of Linear and Non-Linear Methods. *Dyes and Pigments*, **72**, 130-133. <https://doi.org/10.1016/j.dyepig.2005.07.020>
- [51] Ghiaci, M., Abbaspur, A., Kia, R. and Seyedeyn-Azad, F. (2004) Equilibrium Isotherm Studies for the Sorption of Benzene, Toluene, and phenol onto Organo-Zeolites and as-Synthesized MCM-41. *Separation and Purification Technology*, **40**, 217-229. <https://doi.org/10.1016/j.seppur.2004.03.001>
- [52] Vijayaraghavan, K., Padmesh, T.V.N., Palanivelu, K. and Velan, M. (2006) Biosorption of Nickel (II) Ions onto *Sargassum wightii*: Application of Two-Parameter and Three-Parameter Isotherm Models. *Journal of Hazardous Materials*, **133**, 304-308. <https://doi.org/10.1016/j.jhazmat.2005.10.016>
- [53] Kundu, S. and Gupta, A.K. (2006) Arsenic Adsorption onto Iron Oxide-Coated Cement (IOCC): Regression Analysis of Equilibrium Data with Several Isotherm Models and Their Optimization. *Chemical Engineering Journal*, **122**, 93-106. <https://doi.org/10.1016/j.cej.2006.06.002>
- [54] Pérez-Marín, A.B., Zapata, V.M., Ortuno, J.F., Aguilar, M., Sáez, J. and Lloréns, M. (2007) Removal of Cadmium from Aqueous Solutions by Adsorption onto Orange Waste. *Journal of Hazardous Materials*, **139**, 122-131. <https://doi.org/10.1016/j.jhazmat.2006.06.008>
- [55] Demirbas, E., Kobya, M.K.A.E. and Konukman, A.E.S. (2008) Error Analysis of Equilibrium Studies for the Almond Shell Activated Carbon Adsorption of Cr (VI) from Aqueous Solutions. *Journal of Hazardous Materials*, **154**, 787-794. <https://doi.org/10.1016/j.jhazmat.2007.10.094>
- [56] Weber, T.W. and Chakravorti, R.K. (1974) Pore and Solid Diffusion Models for Fixed-Bed Adsorbers. *AIChE Journal*, **20**, 228-238. <https://doi.org/10.1002/aic.690200204>
- [57] Adamson, A.W. and Gast, A.P. (1967) *Physical Chemistry of Surfaces* (Vol. 15). Interscience, New York.
- [58] Zeldowitsch, J. (1934) Adsorption Site Energy Distribution. *Acta Physico-Chimica URSS*, **1**, 961-973.
- [59] Haghseresh, F. and Lu, G.Q. (1998) Adsorption Characteristics of Phenolic Compounds onto Coal-Reject-Derived Adsorbents. *Energy & Fuels*, **12**, 1100-1107. <https://doi.org/10.1021/ef9801165>
- [60] Ghaedi, M., Ansari, A., Habibi, M.H. and Asghari, A.R. (2014) Removal of Malachite Green from Aqueous Solution by Zinc Oxide Nanoparticle Loaded on Activated Carbon: Kinetics and Isotherm Study. *Journal of Industrial and Engineering Chemistry*, **20**, 17-28. <https://doi.org/10.1016/j.jiec.2013.04.031>

- [61] Lagergren, S. (1898) About the Theory of So-Called Adsorption of Soluble Sub-Stances. *Vetenskapsakad. Handlingar* Band, 1-39.
- [62] Ho, Y.S. and McKay, G. (1998) A Comparison of Chemisorption Kinetic Models Applied to Pollutant Removal on Various Sorbents. *Process Safety and Environmental Protection*, **76**, 332-340. <https://doi.org/10.1205/095758298529696>
- [63] Ho, Y.S. (2006) Review of Second-Order Models for Adsorption Systems. *Journal of Hazardous Materials*, **136**, 681-689. <https://doi.org/10.1016/j.jhazmat.2005.12.043>
- [64] Kumar, K.V. and Kumaran, A. (2005) Removal of Methylene Blue by Mango Seed Kernel Powder. *Biochemical Engineering Journal*, **27**, 83-93. <https://doi.org/10.1016/j.bej.2005.08.004>
- [65] Tsai, S.C., Wang, T.H., Li, M.H., Wei, Y.Y. and Teng, S.P. (2009) Cesium Adsorption and Distribution onto Crushed Granite under Different Physicochemical Conditions. *Journal of Hazardous Materials*, **161**, 854-861. <https://doi.org/10.1016/j.bej.2005.08.004>
- [66] El-Wakeel, S.T., El-Tawil, R.S., Abuzeid, H.A.M., Abdel-Ghany, A.E. and Hashem, A.M. (2017) Synthesis and Structural Properties of MnO₂ as Adsorbent for the Removal of Lead (Pb²⁺) from Aqueous Solution. *Journal of the Taiwan Institute of Chemical Engineers*, **72**, 95-103. <https://doi.org/10.1016/j.jtice.2017.01.008>